Bioactive Materials 6 (2021) 2676–2687

Contents lists available at ScienceDirect

Bioactive Materials

journal homepage: www.sciencedirect.com/journal/bioactive-materials

Mussel-inspired nanozyme catalyzed conductive and self-setting hydrogel for adhesive and antibacterial bioelectronics

Zhanrong Jia [a,1], Xuanhan Lv [a,1], Yue Hou [a], Kefeng Wang [b], Fuzeng Ren [c], Dingguo Xu [b], Qun Wang [d], Kelong Fan [e,f], Chaoming Xie [a,**], Xiong Lu [a,*]

[a] Key Lab of Advanced Technologies of Materials, Ministry of Education, School of Materials Science and Engineering, Southwest Jiaotong University, Chengdu, 610031, Sichuan, China
[b] National Engineering Research Center for Biomaterials, Sichuan University, Chengdu, 610064, China
[c] Department of Materials Science and Engineering, Southern University of Science and Technology, Shenzhen, Guangdong, 518055, China
[d] College of Life Science and Biotechnology, Mianyang Teachers' College, Mianyang, 621006, China
[e] CAS Engineering Laboratory for Nanozyme, Key Laboratory of Protein and Peptide Pharmaceuticals, Institute of Biophysics, Chinese Academy of Sciences, Beijing, 100101, China
[f] Nanozyme Medical Center, School of Basic Medical Sciences, Zhengzhou University, Zhengzhou, 450001, China

ARTICLE INFO

Keywords:
Mussel-inspired nanozyme
Adhesive hydrogel
Conductive hydrogel
Antibacterial hydrogel
Bioelectronics

ABSTRACT

Adhesive hydrogels have broad applications ranging from tissue engineering to bioelectronics; however, fabricating adhesive hydrogels with multiple functions remains a challenge. In this study, a mussel-inspired tannic acid chelated-Ag (TA-Ag) nanozyme with peroxidase (POD)-like activity was designed by the *in situ* reduction of ultrasmall Ag nanoparticles (NPs) with TA. The ultrasmall TA-Ag nanozyme exhibited high catalytic activity to induce hydrogel self-setting without external aid. The nanozyme retained abundant phenolic hydroxyl groups and maintained the dynamic redox balance of phenol-quinone, providing the hydrogels with long-term and repeatable adhesiveness, similar to the adhesion of mussels. The phenolic hydroxyl groups also afforded uniform distribution of the nanozyme in the hydrogel network, thereby improving its mechanical properties and conductivity. Furthermore, the nanozyme endowed the hydrogel with antibacterial activity through synergistic effects of the reactive oxygen species generated via POD-like catalytic reactions and the intrinsic bactericidal activity of Ag. Owing to these advantages, the ultrasmall TA-Ag nanozyme-catalyzed hydrogel could be effectively used as an adhesive, antibacterial, and implantable bioelectrode to detect bio-signals, and as a wound dressing to accelerate tissue regeneration while preventing infection. Therefore, this study provides a promising approach for the fabrication of adhesive hydrogel bioelectronics with multiple functions via mussel-inspired nanozyme catalysis.

1. Introduction

Hydrogels are promising candidate materials for implantable and wearable bioelectronics owing to their water-containing chemical structures resembling soft tissues and their tunable mechanical properties such as flexibility and stretchability [1–4]. The currently available hydrogel bioelectronics lack multifunctional characteristics to fully adapt to biological environments. In particular, the lack of self-adhesiveness makes the hydrogel bioelectronics inconvenient and unstable for bio-signal detection, thereby necessitating external aids [5,6]. Hydrogels with strong adhesion capabilities can eliminate the need for external aids, facilitating comfortable wear experience, conformal contact with the tissues, and reliable and stable performance [7–9]. The adhesive hydrogels can be designed by considering the synergistic effects of chemistry, topology, and mechanics [10,11]. Various adhesive hydrogels have been developed based on different adhesion strategies, such as supramolecular-based adhesives, hydrogen bonds, nucleobases, and topological adhesive hydrogels [12–14].

Peer review under responsibility of KeAi Communications Co., Ltd.
* Corresponding author.
** Corresponding author.
E-mail addresses: xie@swjtu.edu.cn (C. Xie), luxiong_2004@163.com (X. Lu).
[1] These authors contributed equally to this work.

https://doi.org/10.1016/j.bioactmat.2021.01.033
Received 26 October 2020; Received in revised form 22 January 2021; Accepted 29 January 2021
2452-199X/© 2021 The Authors. Production and hosting by Elsevier B.V. on behalf of KeAi Communications Co., Ltd. This is an open access article under the CC BY-NC-ND license (http://creativecommons.org/licenses/by-nc-nd/4.0/).

Natural adhesion also inspires for the design of adhesive hydrogels. Many organisms such as marine mussels and sandcastle worms exhibit remarkable adhesion to various materials [15]. Mussel shows strong adhesiveness in seawater via its 3,4-dihydroxyphenylalnine (DOPA)-containing mussel foot proteins. The catechol side chain in DOPA can react with various substrate surfaces via different non-covalent interactions and chemical crosslinking. Inspired by mussel adhesive chemistry, catechol-based molecules, peptides, and polymers have been used to modify material surfaces [16,17]. Our previous studies have demonstrated that adhesive hydrogels can be produced by a mussel-inspired strategy [18]. Based on the studies on mussel-inspired adhesion, it is critical to dynamically control the redox balance between catechol and quinone groups, where a high content of catechol groups is maintained inside the hydrogel networks to provide long-term adhesiveness of the hydrogel [19–22]. In addition to the catechol-based adhesive hydrogels, polyphenol-based hydrogels such as tannic acid (TA)-based hydrogels also exhibit strong adhesiveness through a similar mussel adhesion mechanism [23,24]. Notably, adhesive hydrogels are typically prepared via free-radical polymerization, requiring external stimuli such as UV irradiation or thermal initiation to induce gelation, which limits the their practical applications [25,26]. Therefore, it is imperative to develop new routes for producing adhesive hydrogel bioelectronics, particularly implantable bioelectrodes, which can undergo self-setting by triggering free-radical polymerization without external stimuli under physiological conditions.

Enzymatic catalysis is an environmentally friendly strategy to catalyze radical polymerization to enable the self-setting of hydrogels without external stimuli [27,28]. Enzymes catalyze metabolic reactions and generate biomacromolecules in living cells [29,30]. However, natural enzymes are costly and unstable; therefore, they require restricted conditions to perform catalytic functions. Recently, nanozymes (*i.e.*, nanomaterials with intrinsic enzyme-like characteristics) have attracted significant interest owing to their low cost and high stability [31–33]. Diverse nanozymes based on noble metals, transition metals, and carbon nanomaterials show enzyme-like catalytic properties, including peroxidase, oxidase, catalase, and superoxide dismutase activities [34–37]. In particular, noble metal nanoparticle (NP)-based nanozymes with peroxidase (POD)-like catalytic activity can produce •OH radicals [38,39]. For example, Ag NPs have been used as oxidase nanozymes to trigger the oxidation of *o*-phenylenediamine [40,41]. Importantly, nanozymes not only mimic the catalytic activities of natural enzymes but also exhibit the unique properties of nanomaterials; therefore, they can be used to incorporate and tune the functionalities of hydrogels [42–45]. Recent advances in nanozymes suggest that it is possible to develop a stable and efficient nanozyme to synthesize adhesive hydrogels with multiple functions for bioelectronics.

Notably, metallic NPs with ultrasmall sizes exhibit unique performance on the surface, as well as optical, electrical, magnetic, and catalytic properties [46,47]. Furthermore, we recently found that the phenol-containing lignin-chelated Ag NPs form a dynamic redox system, which can trigger hydrogel gelation and endow it with adhesive properties [48]. An additional study has reported the formation of stable redox pairs based on metal ions and catechols, which can activate ammonium persulfate (APS) to generate free radicals and catalyze hydrogel gelation [49]. Moreover, in the presence of quinone-based electron acceptors (e.g., *p*-benzoquinone), the electrons can be transferred from the Ag NP surface to quinone to induce a partial positive charge on the Ag NP surfaces [48,50,51]. These previous studies suggest that the complexation of polyphenols and ultrasmall metallic nanomaterials is a feasible approach to generate novel nanozymes with catalytic capabilities.

In this study, a mussel-inspired nanozyme was developed by chelating ultrasmall Ag nanoparticles (Ag NPs) with natural polyphenol, TA. The ultrasmall TA-chelated Ag (TA-Ag) nanozyme could catalyze hydrogel self-setting without requiring an external aid. Similar to the adhesion mechanism of the mussel, the ultrasmall TA-Ag nanozyme maintained the dynamic redox balance of phenol-quinone, and therefore endowed the hydrogel with a long-term and repeatable adhesiveness. The nanozyme with phenolic groups was uniformly distributed and interacted with the hydrogel network, thereby affording good mechanical properties and conductivity of the hydrogel, and allowing it to act as an adhesive bioelectrode for detecting physiological signals. Moreover, the hydrogel accelerated the wound regeneration in rats. Additionally, the hydrogel exhibited catalytic dynamic antibacterial activity and effective bacteria adhesion capability, which further intensified its antibacterial activity. The ultrasmall nanozyme-catalyzed adhesive hydrogel with multiple functionalities has versatile applications in fields such as adhesive epidemic biosensors, wearable devices, and medical patches.

2. Results

2.1. Catalytic mechanism of the ultrasmall TA-Ag nanozymes

The ultrasmall TA-Ag nanozyme was generated via reduction of Ag^+ by TA to form TA-chelated Ag NPs, with TA acting as a protective ligand to prevent the aggregation and growth of Ag NPs and maintain the ultrasmall size of the nanozyme (Fig. 1). During the reduction of Ag NPs, a portion of the phenolic hydroxyl groups of TA was oxidized to quinones, which acted as electron acceptors [52]. Thus, the Ag NP and TA formed an electron donor-acceptor complex, and the electrons could be efficiently transferred from the surface of Ag NP to the quinones of TA with the assistance of the localized surface plasmon resonance (LSPR) characteristic of the Ag NPs. The electron transfer between the Ag NPs and TA maintained the dynamic redox balance of phenol-quinone, which enabled the ultrasmall TA-Ag nanozyme to exhibit a high redox activity and stable POD-like catalytic activity (Fig. 1a). In addition, the phenolic hydroxyl groups in this nanozyme showed high affinity to various molecules, serving as adsorption sites to further increase the catalytic efficiency of the nanozyme.

An adhesive and conductive hydrogel was formed via ultrasmall TA-Ag nanozyme-induced self-catalytic polymerization at room temperature (25 °C) without ultraviolet (UV) light irritation or thermal initiation, which was attributed to the catalytic capability of the ultrasmall TA-Ag nanozyme (Fig. 1b). The as-prepared ultrasmall TA-Ag nanozyme solution was mixed with the monomers and initiator (ammonium peroxysulfate, APS), resulting in efficient APS activation to generate radicals and trigger the free-radical polymerization of the monomers, thus yielding the adhesive hydrogel. The catalytic mechanism was based on the continuous electron transfer from the ultrasmall TA-Ag nanozyme to the initiators, which occurred during the conversion of phenol to quinone. Owing to the efficient catalytic activity of the ultrasmall TA-Ag nanozyme, the hydrogel could be catalyzed to self-set in various shapes. This yielded an injectable hydrogel with multi-functionalities at the site of injury, particularly at the subcutaneous sites for laparoscopic placement in clinical settings.

The POD-like catalytic activity of the nanozyme and antibacterial properties of Ag endowed the hydrogel with catalytic dynamic antibacterial activity, which was further enhanced by the bacterial adhesion capability of the phenolic hydroxyl groups in the nanozyme (Fig. 1c). Moreover, the ultrasmall TA-Ag nanozyme maintained the dynamic redox balance of phenol-quinone, which provided sufficient polyphenolic hydroxyl groups inside the hydrogel, and endowed the nanozyme-catalyzed hydrogel with long-term and repeatable adhesiveness (Fig. 1d). The uniform dispersion of the ultrasmall TA-Ag nanozyme in the hydrogel network contributed to the outstanding conductivity and mechanical properties of the hydrogel. Therefore, the hydrogel can be used as an adhesive and flexible bioelectrode to detect physiological signals while preventing infection.

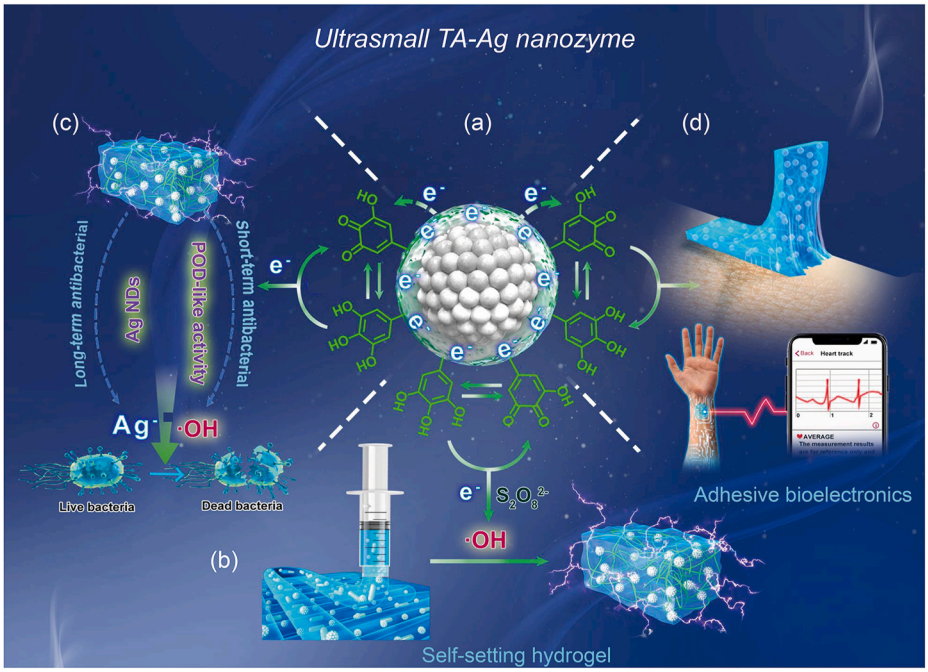

Fig. 1. Catalytic mechanism of the ultrasmall TA-Ag nanozyme. (a) TA-Ag nanozyme is generated by chelating ultrasmall silver nanoparticles (Ag NPs) with tannic acid (TA), where the electron transfer between Ag NP and TA maintains the dynamic redox balance of phenol-quinone. (b) Nanozyme-induced self-setting of the hydrogel. (c) Nanozyme endows the hydrogel with catalytic dynamic antibacterial activity. (d) Dynamic redox balance of phenol-quinone allowing the ultrasmall TA-Ag nanozyme-catalyzed hydrogel to be used as an adhesive and conductive bioelectrode to detect biosignals.

2.2. Characterization of the nanozyme and its catalytic activity

The structure of the ultrasmall TA-Ag nanozyme was examined by transmission electron microscopy (TEM). As shown in Fig. 2a, the nanozyme exhibited an ultrasmall spherical structure with an average diameter of 5 nm. High-resolution TEM (HR-TEM) data showed that the lattice spacing values were 2.3 and 2.0 Å, corresponding to the (1 1 1) and (2 0 0) crystallographic planes of Ag, respectively (Fig. 2a, inset). The X-ray diffraction (XRD) pattern also exhibited the typical diffraction peaks of Ag (Fig. 2b). The X-ray photoelectron spectroscopy (XPS) data revealed the presence of phenol and quinone groups on the Ag NP surfaces, confirming the presence of TA chelates on the Ag core (Fig. S2). The XPS data also show that the Ag 3d peak position of the TA-Ag nanozyme was shifted by 0.17 eV compared with that of the bare Ag NPs (Fig. 2c), indicating an electron-deficient state induced by the quinone-based electron acceptor [51]. These results confirm that the ultrasmall TA-Ag nanozyme was successfully synthesized.

The ultrasmall TA-Ag nanozyme exhibited high POD-like activity, as demonstrated by the catalytic oxidation of the POD substrate, 3,3′,5,5′-tetramethylbenzidine (TMB). After adding the nanozyme to a TMB solution in the presence of H_2O_2, the color changed to blue (Fig. 2d, inset). Moreover, the POD-like activity of the ultrasmall TA-Ag nanozyme was 22 times than that of the pure Ag NPs (Fig. 2d). The specific activities of the TA-Ag nanozyme and Ag were 0.67 and 0.03 units mg^{-1}, respectively. Meanwhile, the nanozyme exhibited high catalytic efficiency and stability in the presence of H_2O_2 at different temperatures (Fig. S3). Additionally, the nanozyme also showed high POD-like activity in the presence of APS, which is essential for catalyzing hydrogel polymerization. The Michaelis–Menten constants (K_M) of the nanozyme for TMB was 2.28 mM in the presence of H_2O_2 (Figs. 2e), and 2.19 mM in the presence of APS (Fig. 2f). The K_M of the nanozyme for H_2O_2 was 180.53 mM (Fig. S4). The generation of •OH radicals plays an important role in the POD-like catalytic systems. To confirm the generation of •OH, 5,5-dimethyl-1-pyrroline N-oxide (DMPO)-trapped electron spin-resonance resonance (ESR) experiments were conducted. The ESR spectra of the TA-Ag nanozyme with H_2O_2 and APS showed a quartet of signals, confirming the presence of •OH (Fig. 2g), which demonstrates that the ultrasmall TA-Ag nanozyme is an efficient POD-like catalyst.

The high catalytic activity of the ultrasmall TA-Ag nanozyme is attributed to the following factors. First, the ultrasmall TA-Ag nanozyme contained phenol-quinone redox pairs on the outer surface, which continuously transferred electrons to the peroxide (Fig. 1a). Second, the core of the Ag NP had an ultrasmall size and therefore exhibited a strong LSPR effect (Fig. S5), and the ultrasmall Ag NP was further activated by the quinone on the outer layer, as indicated by the XPS analysis (Figs. 2c and S2). Thus, the Ag NPs continuously provide electrons to maintain the redox activity of the phenol-quinone pairs.

The electron transfer from the Ag core to the quinone groups of TA on the outer surface was investigated using employing density functional theory (DFT; Fig. 2 h and i). In the Ag (110)-benzoquinone model, the main Ag–O interactions were formed between the Ag atoms and O atoms of the carbonyl groups (Fig. 2h). The electron density difference showed that the electron transfer occurred between benzoquinone and the Ag (110) surface. As shown in Fig. 2i, the red region represents charge accumulation, and the blue region indicates charge depletion. On the Ag (110) surface, charge depletion occurred in the Ag atoms, and charge accumulation was observed in the O atoms of the carbonyl groups (O_{103} and O_{105}) (Fig. 2i), indicating Ag–O interactions between the Ag core and TA. The Mulliken population method was used to quantitatively analyze the change in charge, thereby affording an in-depth understanding of the electron transfer after benzoquinone adsorption on the Ag (110) surface. The changes in the charges calculated by the Mulliken population analysis are listed in Table S12, suggesting electron transfer from the Ag atoms to O atoms and formation of Ag–O interactions. Furthermore, the ultrasmall TA-Ag nanozyme could effectively catalyze hydrogel self-setting without external stimuli (Fig. 2j). The phenol-quinone redox pairs provide electrons to APS to generate radicals, resulting in the rapid *in situ* gelation of the PAA hydrogel. Moreover, the gelation time could be controlled by varying the content of nanozyme or APS (Fig. S6). To demonstrate the universality of the catalytic effects of the nanozyme, it was mixed with a biocompatible monomer solution to form an injectable hydrogel for repairing the full-thickness skin defects in a rat model (Fig. S7) [53–55].

2.3. Catalytic dynamic antibacterial activity of the nanozyme

The ultrasmall TA-Ag nanozyme exhibits rapid short-term and long-term bactericidal activities. The rapid short-term bactericidal activity is

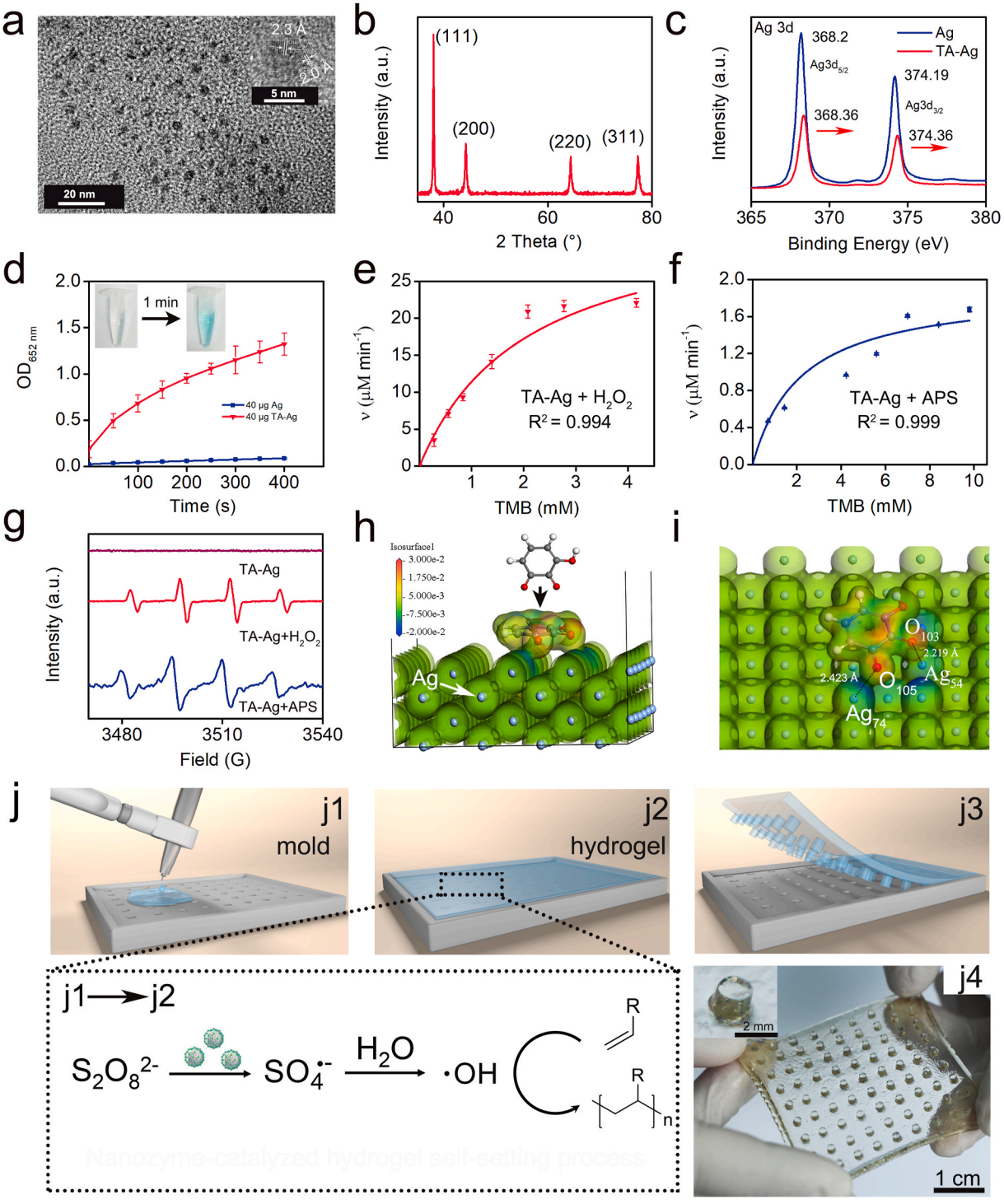

Fig. 2. Characterization and catalytic kinetics of the ultrasmall TA-Ag nanozyme. (a) Transmission electron microscopy (TEM) images of the ultrasmall TA-Ag nanozymes. (b) X-ray diffraction (XRD) pattern of the ultrasmall TA-Ag nanozymes. (c) High-resolution X-ray photoelectron spectroscopy (XPS) data of the Ag 3d regions for Ag NPs and ultrasmall TA-Ag nanozymes. (d) POD-like activities of the ultrasmall TA-Ag nanozymes and Ag NPs; inserted images (tubes) represent the visual color changes of 3,3′,5,5′-tetramethylbenzidine (TMB). Michaelis–Menten curves for the POD-like activity of the ultrasmall TA-Ag nanozyme with varied TMB concentrations in the presence of (e) H_2O_2 and (f) ammonium peroxysulfate (APS). (g) 5,5-dimethyl-1-pyrroline N-oxide (DMPO) spin-trapping electron spin-resonance resonance (ESR) spectra of the ultrasmall TA-Ag nanozyme for H_2O_2 and ammonium persulfate (APS). Density functional theory (DFT) study of 3-hydroxy-1,2-benzoquinone adsorption on the Ag (110) surface; (h) side-view of the three-dimensional plots of the electron density difference with an isovalue of 0.20 e Å^{-3}; (i) top view. Bond lengths are in angstrom (Å) units. Charge accumulation and charge depletion are represented by red and blue, respectively. (j) Schematic of the TA-Ag-based hydrogel self-setting in a mold; (j1) pre-polymerization solution of the hydrogel was injected into a mold; (j2) injectable hydrogel self-set through nanozyme catalyzation; (j3) the hydrogel was exfoliated from the mold; (j4) digital photograph of the self-set TA-Ag-PAA hydrogel with cylindrical micropatterns.

attributed to the catalytic dynamic antibacterial activity of the ultrasmall TA-Ag nanozyme, based on the generation of reactive oxygen species (ROS) in the POD-like catalytic reactions. In the presence of H_2O_2, the ultrasmall TA-Ag nanozyme with POD-like catalytic activity can rapidly generate •OH radicals, leading to the inactivation of bacteria. The bacterial adhesion of the ultrasmall TA-Ag nanozyme facilitated its immobilization on the bacteria, which shortened the diffusion distance of ROS to bacteria and strengthened the bactericidal effect of the ROS (Fig. 3a).

The rapid short-term antibacterial activity was demonstrated using the co-culture of the ultrasmall TA-Ag nanozyme with two bacterial taxa, gram-negative *Escherichia coli (E. coli)* and gram-positive

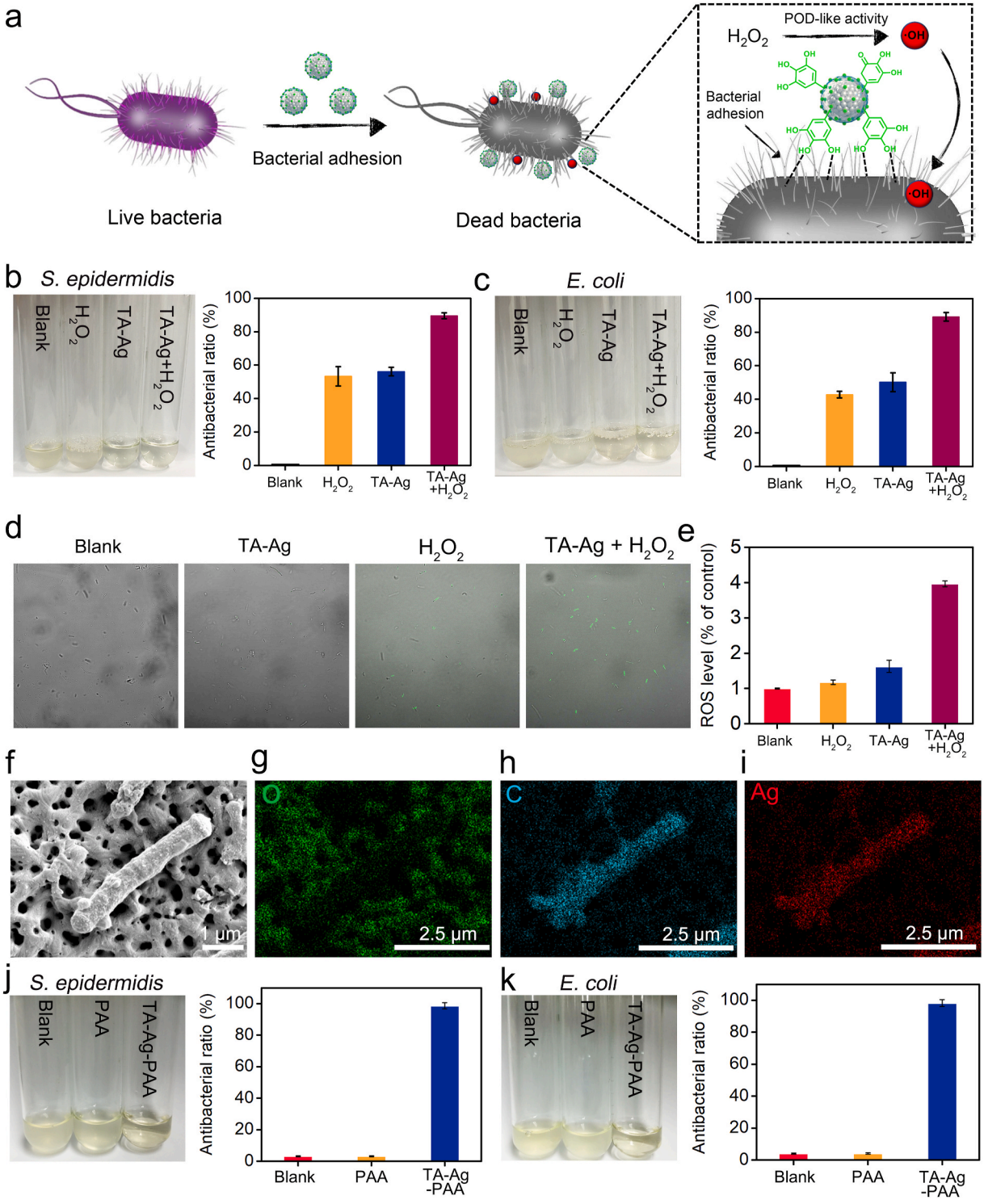

Fig. 3. Antibacterial activity of the ultrasmall TA-Ag nanozyme. (a) Ultrasmall TA-Ag nanozyme kills bacteria via adhesion on the bacterial surface and generation of reactive oxygen species (ROS) by enzyme-like catalysis. (b–c) Photographs and bactericidal ratios after the different treatments for 2 h. (d) Confocal laser scanning microscopy (CLSM) images and (e) the semi-quantitative determination of the fluorescence signal of *E. coli* cells stained by DCFH-DA/HPF. (f–i) SEM image and elemental mapping of *E. coli* cells co-cultured with the ultrasmall TA-Ag nanozyme. (j–k) Photographs and bactericidal ratio of the nanozyme-incorporated hydrogels (0.18 wt%) co-cultured with *S. epidermidis* and *E. coli.* solution after one day.

Staphylococcus epidermidis (S. epidermidis). The bacterial suspensions of TA-Ag nanozyme in the presence of H_2O_2 were clear (Fig. 3b and c, left). Moreover, in the presence of H_2O_2, the antibacterial ratios of TA-Ag nanozyme reached 90% to *S. epidermidis*, and 89% to *E. coli* in 2 h (Fig. 3b and c, right). Intracellular ROS levels were measured, which is relevant to the bacterial death that is caused by oxidative stress. The cellular •OH level was detected using hydroxyphenyl fluorescein after culturing with different groups for 35 min (Fig. 3d and e) [56]. In the nanozyme group in the presence of H_2O_2, bright green fluorescence signals were observed in the bacteria. The H_2O_2 groups presented slight green fluorescence signals due to the partial self-decomposition of H_2O_2. In contrast, no intense fluorescence signals were observed in the other groups. These results indicate that ultrasmall TA-Ag nanozymes exhibit effective POD-like activity in antibacterial tests.

Notably, the diffusion distances and lifetimes of ROS are generally limited in the biological environments. The bacterial adhesion of the ultrasmall TA-Ag nanozyme facilitated its immobilization on bacteria and enhanced the bactericidal effect of the ROS (Fig. 3a). The ultrasmall TA-Ag nanozyme exhibited a good bacterial adhesion capability and thereby increasing the bactericidal efficiency of ROS. As shown in Fig. 3f–i, a substantial portion of the nanozyme was attached to the bacterial surfaces and better antibacterial activity was observed compared to that of the Ag NPs (Fig. S8). The superior adhesion capability is attributed to the phenolic hydroxyl groups on the nanozyme, which can form various interactions with the bacterial cell membranes [57]. Thus, ROS generation and bacterial-adhesion capability of the ultrasmall TA-Ag nanozyme synergistically resulted in an efficient and rapid antibacterial activity.

Long-term antibacterial activity results from the intrinsic bactericidal activity of the Ag NPs. Ag nanomaterials are well-known broad-spectrum antibacterial agents that kill the bacteria by disrupting their membranes [58]. The images of the bacterial suspensions co-cultured with the nanozyme-incorporated hydrogels after 24 h are shown in Fig. 3j and k. The suspensions cultured with the polyacrylic acid (PAA) hydrogel appeared turbid. In contrast, those cultured with the nanozyme-incorporated (TA-Ag-PAA) hydrogel were clear, indicating that most of the bacteria were killed. Quantitative analysis indicated that the bactericidal ratios of the TA-Ag-PAA hydrogel for *E. coli* and *S. epidermidis* after one day were 98.2% and 98.5%, respectively. In general, the TA-Ag-PAA hydrogel showed effective inhibitory activity toward both gram-negative and gram-positive bacteria.

2.4. Adhesiveness of the nanozyme-incorporated hydrogel

The TA-Ag-PAA hydrogel exhibited self-adhesiveness, and could repeatedly adhere to various surfaces for a long duration. As shown in Fig. 4a, the hydrogel could adhere to various surfaces, including cherry tomatoes, glass bottles, mouse livers, and metal nuts. Quantitative tensile-adhesion test results showed that the adhesive strengths of the hydrogel to glass, titanium, polytetrafluoroethylene (PTFE), and porcine skin are 35, 45, 54, and 26 kPa, respectively (Fig. 4b). Furthermore, the hydrogel strongly adhered to porcine skin even after 30 cycles of the stripping-adhesion test, indicating its repeatable and long-term adhesiveness (Fig. 4c). It could also be repeatedly adhered to and stripped off from human skin without any harm or irritation (Fig. 4d), which is crucial for bioelectronic applications.

Repeatable and long-term adhesiveness is attributed to the dynamic phenol-quinone redox system formed by the ultrasmall TA-Ag nanozyme inside the hydrogel network, which provides sufficient phenolic hydroxyl groups for adhesion (Fig. 4e). Notably, the repeatable and long-term adhesion of the mussels in nature is also based on the dynamic redox system involving a set of mussel foot proteins (Mfps) in the byssal thread (Fig. 4e–i). Mfp-3 and Mfp-6 significantly contribute to mussel adhesion. Mfp-6, which has a cysteine residue, acts as a reductant to

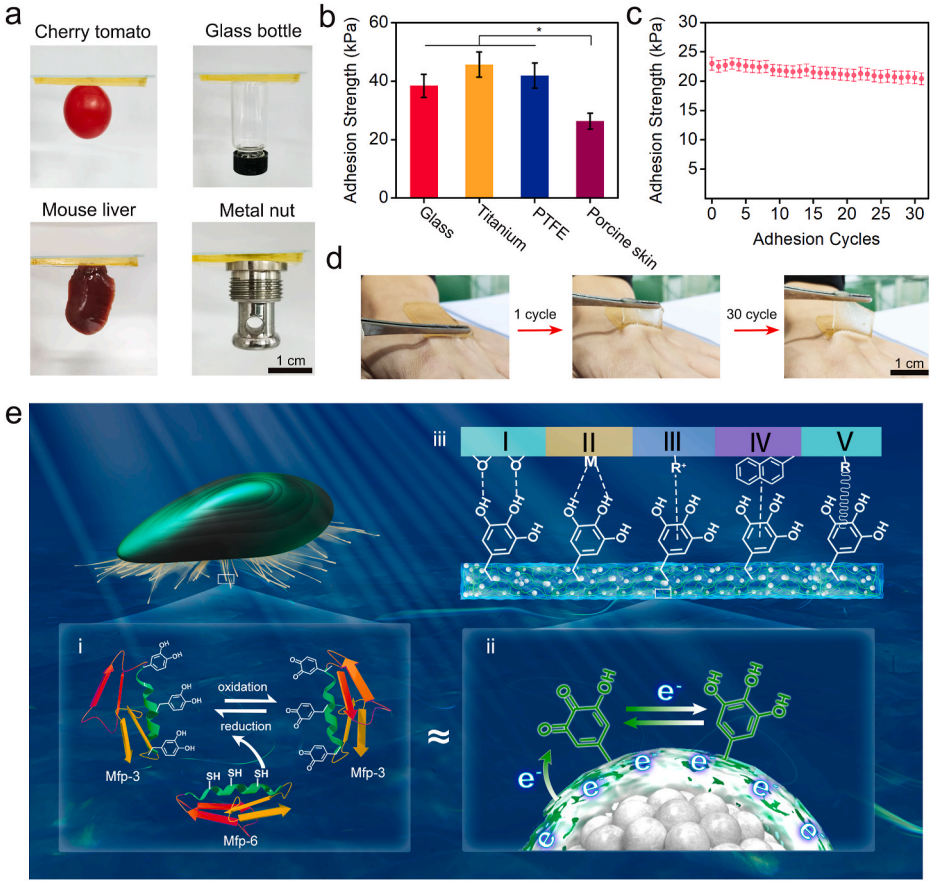

Fig. 4. Adhesive performance of TA-Ag-PAA hydrogel. (a) Hydrogel adhered to various surfaces (the content of TA-Ag nanozyme is 0.22 wt%). (b) The adhesive strength of the hydrogels to different substrates. (c) The repeatable adhesive strength of the hydrogel to porcine skin tissue. (d) Long-term adhesion of the hydrogel to human skin tissue after 30 cycles without causing irritation. (e) Mussel-inspired adhesion mechanism of the hydrogel; (i) mussel adhesion; (ii) ultrasmall TA-Ag nanozyme creates a redox environment inside the hydrogel and maintains phenolic hydroxyl groups for long-lasting adhesion; (iii) interactions between the hydrogel and various substrates; I. Hydrogen bond. II. Coordination bond. III. Cation–π interaction. IV. π–π interaction. V. Covalent linkage.

prevent the over-oxidation of catechols to quinones to prevent the loss of adhesion [19,59,60]. Inspired by this mechanism, we previously demonstrated that hydrogels with long-term and repeatable adhesion could be achieved by controlling the oxidation of the catechol groups, and the redox balance between the catechol and quinone groups was one of the main factors affecting the adhesive performance of the hydrogels [61].

In this nanozyme-triggered dynamic redox system, Ag NP acts as an electron donor owing to the presence of quinone-based electron acceptor (TA) and the LSPR effect. LSPR is a key property of noble metal NPs, such as Au, Ag, and Cu NPs, which allows electron transfer because of the collective oscillation of free electrons in metal NPs [62]. Chelation with TA further activates ultrasmall Ag NPs and facilitates electron transfer [63]. Therefore, the TA and LSPR allowed the Ag NPs to act as electron donors to the quinone groups, which maintained the redox balance of the phenol/quinone groups (Fig. 4e–ii). In other words, within the nanozyme, the phenolic hydroxyl groups prevented the oxidation of Ag during *in situ* reduction, while the Ag NPs serve as efficient sources of electrons to maintain the redox balance of the phenol/quinone groups. Thus, abundant phenolic hydroxyl groups were retained inside the hydrogel, enabling long-term and repeatable adhesion of the hydrogel to various substrates via hydrogen bonding, coordination bonding, cation-π interactions, π-π interactions, and covalent linkage (Fig. 4e–iii) [64].

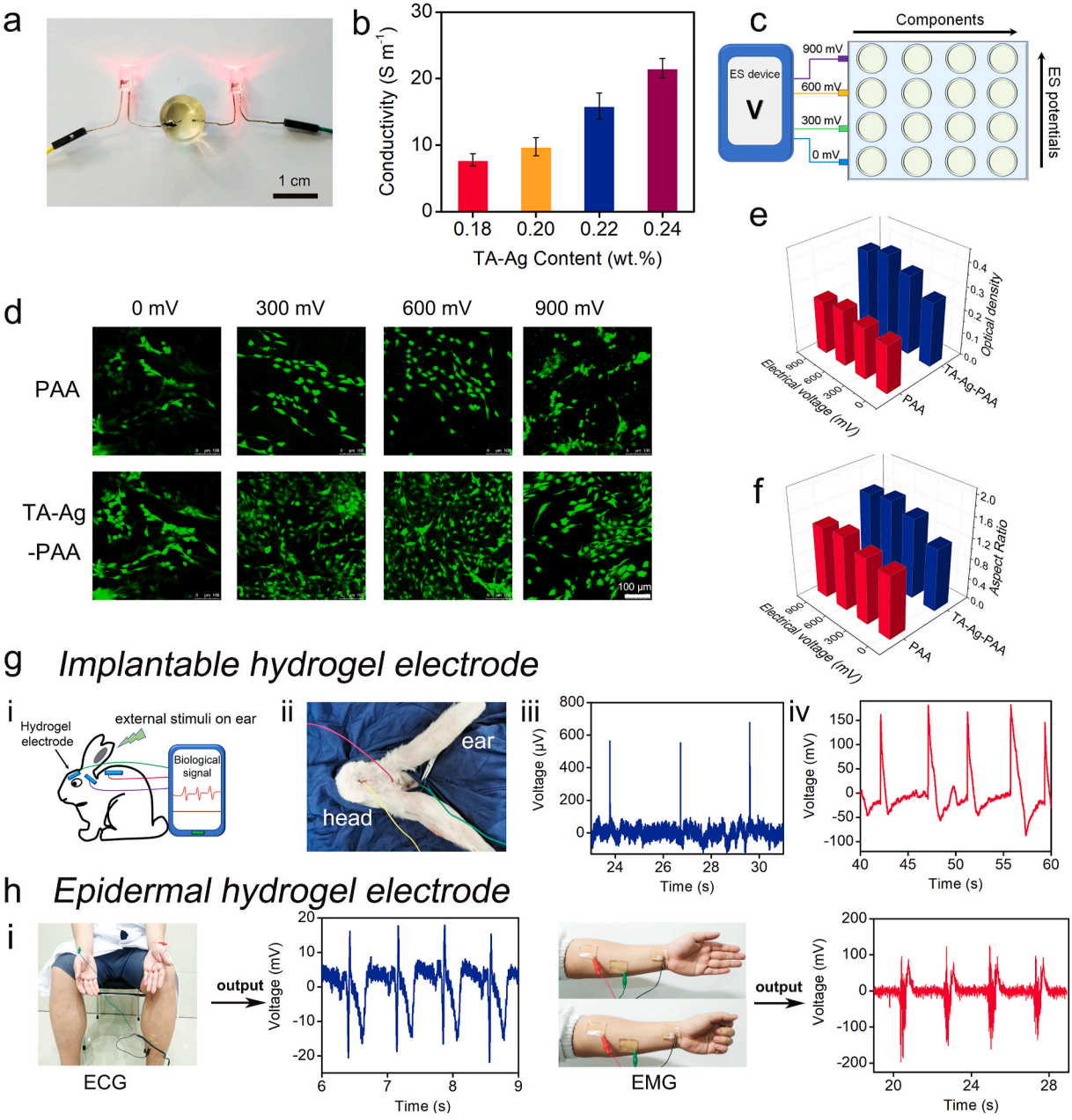

Fig. 5. Conductivity and bioelectronic applications of the TA-Ag-PAA hydrogel. (a) Photographs demonstrating the good conductivity of the hydrogel. (b) The conductivity of the hydrogel as a function of TA-Ag content. (c) High-throughput electrical stimulation of C2C12 cells on the hydrogels. (d) CLSM images of C2C12 myoblasts after three days of culturing. (e) Cell proliferation. (f) Aspect ratio. (g) Hydrogel acting as an implantable electrode in a rabbit's head to measure electromyographic (EMG) signals; (i) Schematic of the sites of the electrodes and external stimuli; (ii) surgical operation; (iii) EMG signals when the rabbit is subjected to a weak current stimulus; (iv) EMG signals when the ear of the rabbit is pressed. (h) Hydrogel acting as an epidermal electrode on human skin to detect (i) electrocardiogram (ECG) and (ii) EMG signals.

2.5. Conductivity and bioelectronic applications

The TA-Ag-PAA hydrogel exhibited excellent conductivity because the ultrasmall TA-Ag nanozyme functioned as a conductive nanofiller in the PAA network. As shown in Fig. 5a, the hydrogel as integrated into a circuit to light up light-emitting diodes (LEDs). The conductivity increased with an increase in the TA-Ag content, affording a maximum value of 21 S m^{-1} (Fig. 5b).

The TA-Ag-PAA hydrogel exhibited good cell affinity and promoted cell adhesion and proliferation via the phenolic hydroxyl groups of the ultrasmall TA-Ag nanozymes. The cell affinity and conductivity could affect the cell behaviors on the hydrogels via phenolic hydroxyl groups and electrical signaling under electrical stimulation (ES) (Fig. 5c). As observed by confocal laser scanning microscopy (CLSM), the C2C12 cells on the TA-Ag-PAA hydrogel showed better adhesion and spreading than those on the PAA hydrogel (Fig. 5d). Under ES, the cells prefer to adhere to the conductive hydrogels at a potential of 300 or 600 mV. However, the cell count decreased to 900 mV, indicating that the high voltage was damaging. Cell proliferation on the hydrogel was further evaluated using the MTT (3-[4,5-dimethylthiazol-2-yl]-2,5-diphenyl tetrazolium bromide) assay (Fig. 5e). Cell proliferation on the TA-Ag-PAA hydrogels was higher than that on the PAA hydrogels, demonstrating that the ultrasmall TA-Ag nanozymes in the hydrogel exhibited no cytotoxicity. The cells exhibited the highest proliferation activity under ES at 600 mV. In addition, the cells on the conductive hydrogels had a high aspect ratio, indicating that the conductive hydrogels favored the earliest stage of myotube formation (Fig. 5f). These results suggest that the phenolic hydroxyl groups and electrical signals show synergistic effects on cell behavior, and the hydrogel provides a platform to tune cell activity.

The combination of biocompatibility, adhesiveness, and conductivity allows the hydrogel to be used as an implantable bioelectrode. As shown in Fig. 5g–i-ii, the wire-connected hydrogel electrodes were implanted in the dorsal muscle of the rabbits to detect the electromyographic (EMG) signals under different conditions. The EMG signals were clearly detected after the application of ES and pressure on the ear (Fig. 5g–iii-iv). The hydrogel electrodes were also attached to the human skin to detect the electrocardiogram (Fig. 5h-i) and EMG signals (Fig. 5h-ii).

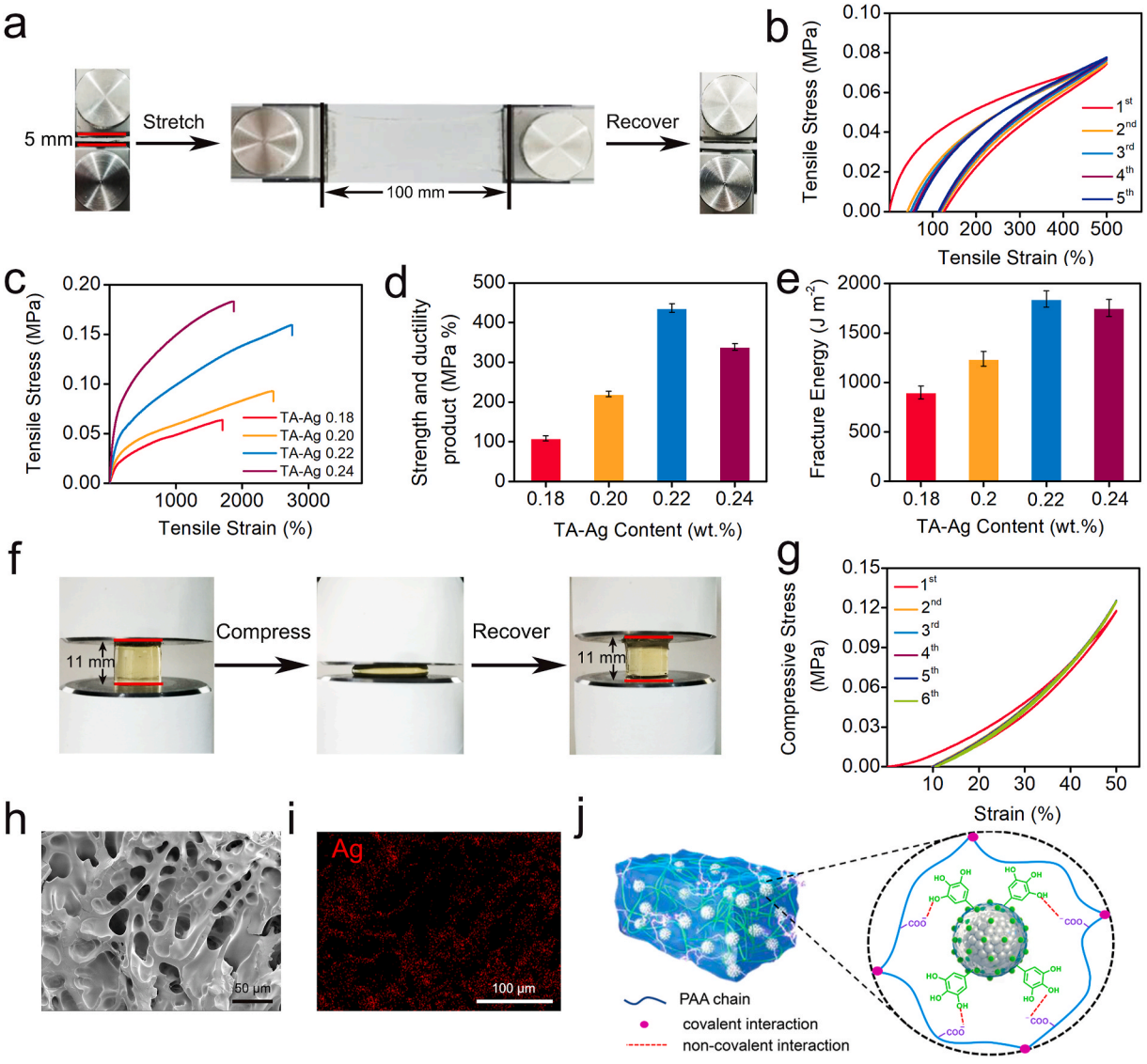

Fig. 6. Mechanical properties of TA-Ag-PAA hydrogels. (a) TA-Ag-PAA hydrogel is elongated to 20 times its initial length and recovered. (b) Cyclic tensile loading–unloading curves of TA-Ag-PAA hydrogel. (c) Typical tensile stress–strain curves. (d) Strengths and ductility products and (e) fracture energies of various hydrogels. (f) Compressive recovery performance of the TA-Ag-PAA hydrogel. (g) Cyclic compressive loading–unloading curves of the TA-Ag-PAA hydrogel. (h) SEM image and (i) Ag elemental mapping of dried TA-Ag-PAA hydrogel. (j) Schematic of the ultrasmall TA-Ag nanozyme-reinforced TA-Ag-PAA hydrogel.

2.6. Mechanical properties of nanozyme-reinforced hydrogels

The TA-Ag-PAA hydrogel exhibited outstanding stretchability, resilience, and toughness, which ensured a mechanical match between the tissues and bioelectronics. As shown in Fig. 6a, the hydrogel could be stretched to 20 times its initial length without breaking and recovers to its original length. The TA-Ag-PAA hydrogel showed a small hysteresis during the loading–unloading cycles, indicating excellent tensile recoverability (Fig. 6b). The stress–strain curves of the TA-Ag-PAA hydrogels indicate that the ultrasmall TA-Ag nanozyme is an important determinant of the mechanical properties of the hydrogels (Fig. 6c). The strengths and ductility products of various hydrogels were measured (Fig. 6d), and the hydrogel with 0.22 wt% TA-Ag exhibited the highest value (436 MPa%) of strength and ductility products. The fracture energy was 1845 J m^{-2}, as determined by the single-edge notched tensile testing, when the ultrasmall TA-Ag nanozyme content of the hydrogel was 0.22 wt% (Fig. 6e). Furthermore, the hydrogel could also withstand a compressive deformation of 85%, and rapidly and fully recovers its initial shape after the pressure was removed (Fig. 6f). The compressive loading–unloading stress–strain curves further showed excellent recoverability of the hydrogel has after six cycles (Fig. 6g). The maximum compression strength was 2.2 MPa (Fig. S9).

The good mechanical performance of the nanozyme-incorporated hydrogel is mainly attributed to two factors. First, the ultrasmall TA-Ag nanozyme was uniformly distributed in the polymer network and acted as a reinforcing nanofiller to strengthen the hydrogel. As demonstrated by scanning electron microscopy and energy-dispersive X-ray spectroscopy mapping, the ultrasmall TA-Ag nanozymes were uniformly distributed in the hydrogel matrix (Fig. 6h and i) and seamlessly integrated with the hydrogel network. Second, TA formed noncovalent dynamic crosslinking interactions with the PAA network, which efficiently dissipated the energy when enduring a large deformation (Fig. 6j). Therefore, the hydrogel exhibits excellent mechanical properties, which can be tuned by controlling the ultrasmall TA-Ag nanozyme content.

2.7. Nanozyme-reinforced hydrogels as wound repair patches

The nanozymes with abundant phenolic groups enable the hydrogel to integrate with the surrounding tissues and act as wound repair patches. An *in vivo* model of the full-thickness skin defects was used to evaluate tissue regeneration with TA-Ag-PAA hydrogel treatment

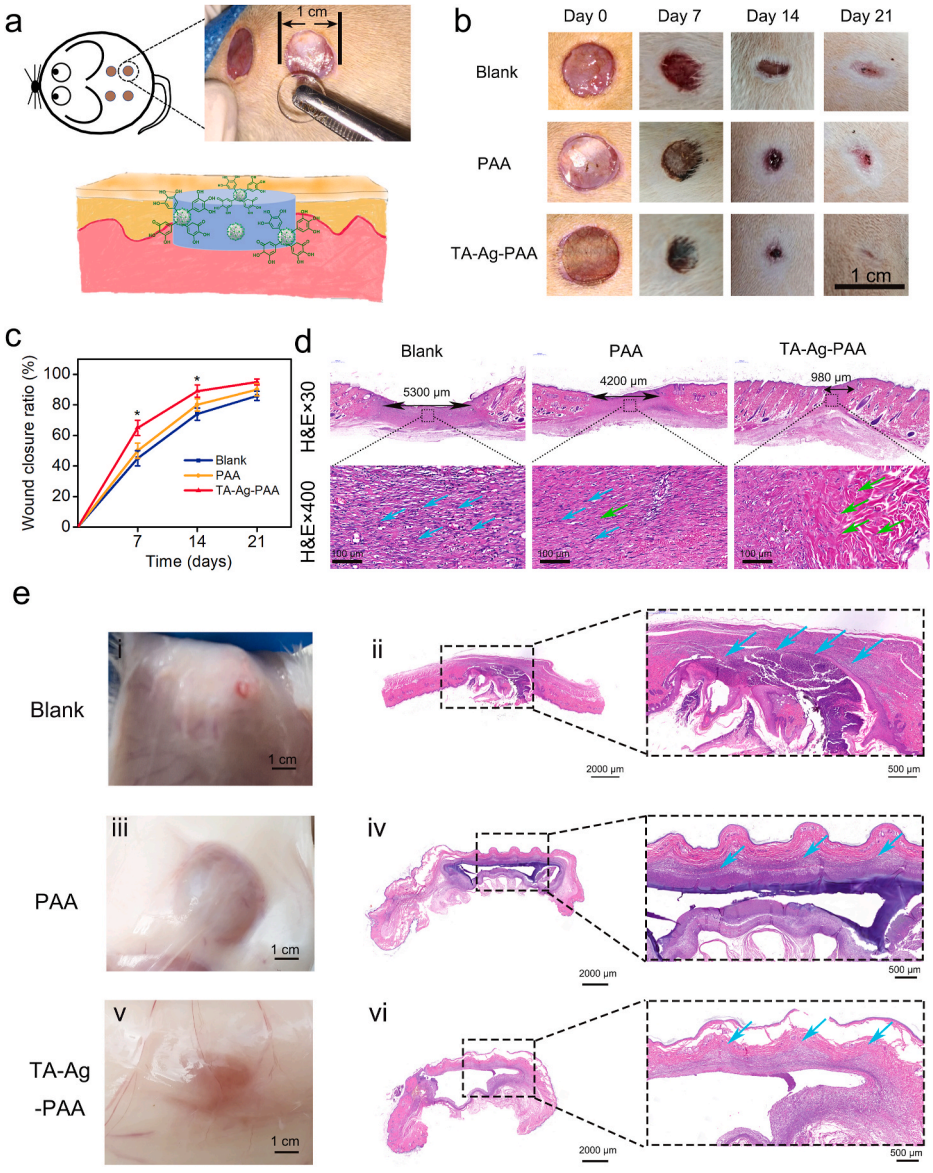

Fig. 7. *In vivo* wound healing with nanozyme-incorporated hydrogel treatment. (a) Schematic of the surgical operation. (b) Digital images and (c) wound closure ratio of the defects with different treatments. (d) Representative images of H&E-stained histological sections after 21 d. The blue arrow indicates edema tissue, and the green arrow indicates the granulation tissue. (e) *In vivo* antibacterial evaluation of the hydrogel; (e–i) Blank group without hydrogels; (e-ii) H&E-stained sections of the connective tissues; (e-iii) Bacterial infection of the PAA hydrogel in the presence of *E. coli* during implantation; (e-iv) H&E-stained sections of the connective tissues surrounding the hydrogel; (e–v) good *in vivo* bactericidal activity of the TA-Ag-PAA hydrogel; (e-vi) H&E-stained sections; the blue arrow indicates multicellular giant cells.

(Fig. 7a). As shown in Fig. 7b, healing was more efficient with the TA-Ag-PAA hydrogel than with the PAA hydrogel or blank groups without the hydrogels. After implantation for 21 days, the wound defect was effectively healed and almost closed in the TA-Ag-PAA hydrogel group, which can be explained by the high tissue affinity of the phenolic hydroxyl groups on the ultrasmall TA-Ag nanozymes. The wound healing rate was evaluated based on the skin wound closure ratio, and the result showed that the wound closure ratio of the TA-Ag-PAA hydrogel was significantly higher than blank groups at initial healing period (Fig. 7c).

Hematoxylin and eosin (H&E) staining was used to evaluate the quality of tissue regeneration in the defects after hydrogel administration. As shown in Fig. 7d, a complete layer of the newly regenerated epidermis was observed in all groups. In the TA-Ag-PAA hydrogel group, the proportion of the new tissue is low. However, in the blank and PAA hydrogel groups, a large immature tissue area was observed. Based on the histological micrographs at high magnification, the collagen fibers were observed in the regeneration area in the TA-Ag-PAA hydrogel groups, while a large number of granulation tissues were observed in the regeneration area of the blank and PAA hydrogel groups. In summary, the TA-Ag-PAA hydrogel can promote wound healing and skin tissue regeneration. The good biocompatibility of the hydrogel is attributed to two factors. First, the phenolic hydroxyl groups coordinated with the Ag NPs to afford a uniform distribution of the ultrasmall TA-Ag nanozyme, thereby reducing the cytotoxicity of Ag. Second, the presence of phenolic hydroxyl groups on the nanozyme surface promoted cell adhesion and proliferation and increased the tissue affinity.

Antibacterial activity is necessary for hydrogel bioelectronics owing to the serious risk of bacterial infections associated with implantable devices for long-term use. The TA-Ag-PAA hydrogels exhibit both rapid and long-term antibacterial activities because of the presence of ultrasmall TA-Ag nanozyme. The antibacterial activity of the TA-Ag-PAA hydrogel was also investigated *in vivo* in a rat model through subcutaneous implantation in the presence of *E. coli* (1 mL, 10^5 cells mL^{-1}) (Fig. 7e). After seven days, the surgical sites were harvested to examine the infections and inflammatory reactions. The blank and PAA hydrogel groups showed purulent infections (Fig. 7e–i and e-iii), whereas the TA-Ag-PAA group had a clear appearance (Fig. 7e–v). The tissues surrounding the hydrogels were excised and stained with hematoxylin and eosin to evaluate the antibacterial properties of the hydrogels. Histological staining showed that the presence of a large number of multinucleated giant cells and edema in the tissues surrounding of the blank (Fig. 7e–ii) and PAA hydrogel groups (Fig. 7e–iv), suggesting that *E. coli* causes a serious inflammatory reaction. In contrast, there were a few multicellular giant cells or edematous tissues in the tissues surrounding the TA-Ag-PAA hydrogel, and a new tissue growth was observed (Fig. 7e–vi). These results further confirmed that the TA-Ag-PAA hydrogels possess good antibacterial properties *in vivo*.

3. Conclusion

A mussel-inspired TA-Ag nanozyme with ultrasmall size was developed via the *in situ* reduction of Ag NPs using TA. The ultrasmall TA-Ag nanozyme shows a high POD-like activity and can effectively produce free radicals. The phenolic hydroxyl groups of TA not only protect and stabilize the nanozyme during synthesis, but also perform a myriad of other functions, making this nanozyme superior to the bare metallic or metal oxide nanozymes. Notably, nano Ag with catalytic properties has been reported, but the catalytic efficiency of the bare nano Ag is very low for use as a nanozyme. This mussel-inspired strategy significantly improves the catalytic efficiency of nano Ag, allowing it to be used as an artificial nanozyme.

As a proof of concept, a conductive, antibacterial, and adhesive hydrogel was prepared using the ultrasmall TA-Ag nanozyme to trigger gelation without requiring external stimuli. Nanozyme-based self-setting hydrogels are employed for the *in situ* repair of irregular wounds, without external stimuli, under physiological conditions in clinical settings. Similar to the mussel adhesion mechanism, the ultrasmall TA-Ag nanozyme maintains a dynamic redox balance of the phenol-quinone groups in the hydrogel network and affords long-term adhesiveness to the hydrogel. The phenolic hydroxyl groups ensure a uniform distribution of the nanozyme inside the hydrogel network, which promotes the interaction between the nanozyme and molecular chains of the hydrogels and consequently improves the conductivity and mechanical properties of the hydrogel. The high POD-like activity and bacterial adhesion capability of the nanozyme also afforded antibacterial properties.

Accordingly, the ultrasmall TA-Ag nanozyme-based hydrogel has been successfully used as an antibacterial wound dressing, self-adhesive biosensor, or implantable and wearable electronic appliance that can directly adhere to biological surfaces for body signal detection. This mussel-inspired nanozyme-based strategy provides a basis for the development of other artificial enzyme-driven hydrogels with diverse applications, such as injectable hydrogels, 3D printed hydrogels, flexible sensors, and bioelectronics.

4. Experimental section

4.1. Materials

Acrylic acid (AA), ammonium persulfate (APS), N,N′-methylene bis acrylamide (BIS), tannic acid (TA) and N,N,N′,N’-tetramethylethylenediamine (TEMED) were purchased from Sigma-Aldrich (St Louis, MO, USA). Silver nitrate (I) was purchased from KESHI Chemical Works in Chengdu, China. 3,3,5,5-tetramethylbenzidine (TMB) was purchased from Sigma-Aldrich. H_2O_2 was purchased from KESHI Chemical Works in Chengdu. All the other reagents and solvents were of reagent grade.

4.2. Preparation of the TA-Ag nanozyme

First, an aqueous solution of TA at a concentration of 2 mg mL^{-1} was prepared by dissolving the weighed amount of TA powder in deionized water with the aid of ultrasonic agitation (solution A). Second, $AgNO_3$ with concentrationS of 1.8, 2.0, 2.2 and 2.4 mg mL^{-1} were added to the solution A and stirred simultaneously for 30 min (solution B). Finally, solution B was centrifuged and washed to obtain the TA-Ag nanozyme. Characterization of the TA-Ag nanozyme is listed in the Supporting Information.

4.3. Preparation of hydrogels

First, AA (2.7 mL), BIS (300 μL, 0.01 g mL^{-1}), APS (1 mL, 0.02 g mL^{-1}) and deionized water (4 mL) were added to the 1 mL of TA-Ag nanozyme solution (0.018, 0.02, 0.022 and 0.024 g mL^{-1}) with simultaneous stirring. After stirring for a few seconds, the monomers were polymerized to the hydrogels. The details of the preparation and characterizations of various hydrogels are listed in the Supporting Information.

CRediT authorship contribution statement

Zhanrong Jia: Methodology, Validation, Formal analysis, Investigation, Data curation, Writing - original draft. **Xuanhan Lv:** Methodology, Investigation. **Yue Hou:** Methodology. **Kefeng Wang:** Methodology. **Fuzeng Ren:** Methodology. **Dingguo Xu:** Methodology, Software. **Qun Wang:** Methodology, Software. **Kelong Fan:** Validation, Methodology. **Chaoming Xie:** Conceptualization, Methodology, Writing - review & editing, Project administration, Funding acquisition. **Xiong Lu:** Conceptualization, Methodology, Writing - review & editing, Project administration, Funding acquisition.

Declaration of competing interest

The authors declare no conflict of interest.

Acknowledgements

This work was financially supported by the National Key Research and Development Program of China (2016YFB0700800), Key-Area Research and Development Program of Guang Dong Province (2019B010941002), NSFC (82072071, 82072073), Fundamental Research Funds for the Central Universities (2682020ZT79), Sichuan Science and Technology Program (2020YJ0009), Young Scientific and Technological Innovation Research Team Funds of Sichuan Province (20CXTD0106). The authors wish to acknowledge the assistance on materials characterization received from Analytical & Testing Center of the Southwest Jiaotong University.

Appendix A. Supplementary data

Supplementary data to this article can be found online at https://doi.org/10.1016/j.bioactmat.2021.01.033.

References

[1] H. Yuk, B. Lu, X. Zhao, Hydrogel bioelectronics, Chem. Soc. Rev. 48 (2019) 1642–1667.
[2] Y. Liu, T. Yang, Y. Zhang, G. Qu, S. Wei, Z. Liu, T. Kong, Ultrastretchable and wireless bioelectronics based on all-hydrogel microfluidics, Adv. Mater. 31 (2019) 1902783.
[3] S. Zhang, Y. Chen, H. Liu, Z. Wang, H. Ling, C. Wang, J. Ni, B. Çelebi-Saltik, X. Wang, X. Meng, Room-temperature-formed pedot: pss hydrogels enable injectable, soft, and healable organic bioelectronics, Adv. Mater. 32 (2020) 1904752.
[4] J. Chen, Q. Peng, T. Thundat, H. Zeng, Stretchable, injectable, and self-healing conductive hydrogel enabled by multiple hydrogen bonding toward wearable electronics, Chem. Mater. 31 (2019) 4553–4563.
[5] C. Xie, X. Wang, H. He, Y. Ding, X. Lu, Mussel-inspired hydrogels for self-adhesive bioelectronics, Adv. Funct. Mater. 30 (2020), 1909954.
[6] D. Gan, Z. Huang, X. Wang, L. Jiang, C. Wang, M. Zhu, F. Ren, L. Fang, K. Wang, C. Xie, Graphene oxide-templated conductive and redox-active nanosheets incorporated hydrogels for adhesive bioelectronics, Adv. Funct. Mater. 30 (2020) 1907678.
[7] X. Liu, J. Liu, S. Lin, X. Zhao, Hydrogel machines, Mater. Today 36 (2020) 102.
[8] G. Ge, Y. Lu, X. Qu, W. Zhao, Y. Ren, W. Wang, Q. Wang, W. Huang, X. Dong, Muscle-inspired self-healing hydrogels for strain and temperature sensor, ACS Nano 14 (2019) 218–228.
[9] S. Baik, H.J. Lee, D.W. Kim, J.W. Kim, Y. Lee, C. Pang, Bioinspired adhesive architectures: from skin patch to integrated bioelectronics, Adv. Mater. 31 (2019) 1803309.
[10] J. Yang, R. Bai, B. Chen, Z. Suo, Hydrogel adhesion: a supramolecular synergy of chemistry, topology, and mechanics, Adv. Funct. Mater. 30 (2020) 1901693.
[11] J.H. Ryu, H.J. Kim, K. Kim, G. Yoon, Y. Wang, G.S. Choi, H. Lee, J.S. Park, Multipurpose intraperitoneal adhesive patches, Adv. Funct. Mater. 29 (2019) 1900495.
[12] J. Yang, R. Bai, Z. Suo, Topological adhesion of wet materials, Adv. Mater. 30 (2018) 1800671.
[13] X. Liu, Q. Zhang, G. Gao, Bioinspired adhesive hydrogels tackified by nucleobases, Adv. Funct. Mater. 27 (2017) 1703132.
[14] C. Cui, C. Fan, Y. Wu, M. Xiao, T. Wu, D. Zhang, X. Chen, B. Liu, Z. Xu, B. Qu, Water-triggered hyperbranched polymer universal adhesives: from strong underwater adhesion to rapid sealing hemostasis, Adv. Mater. 31 (2019) 1905761.
[15] B.K. Ahn, Perspectives on mussel-inspired wet adhesion, J. Am. Chem. Soc. 139 (2017) 10166–10171.
[16] G. Pan, S. Sun, W. Zhang, R. Zhao, W. Cui, F. He, L. Huang, S.-H. Lee, K.J. Shea, Q. Shi, H. Yang, Biomimetic design of mussel-derived bioactive peptides for dual-functionalization of titanium-based biomaterials, J. Am. Chem. Soc. 138 (2016) 15078–15086.
[17] M. Krogsgaard, V. Nue, H. Birkedal, Mussel-inspired materials: self-healing through coordination chemistry, Chem. Eur J. 22 (2016) 844–857.
[18] L. Han, X. Lu, M. Wang, D. Gan, W. Deng, K. Wang, L. Fang, K. Liu, C.W. Chan, Y. Tang, A mussel-inspired conductive, self-adhesive, and self-healable tough hydrogel as cell stimulators and implantable bioelectronics, Small 13 (2017) 1601916.
[19] J. Yu, W. Wei, E. Danner, R.K. Ashley, J.N. Israelachvili, J.H. Waite, Mussel protein adhesion depends on interprotein thiol-mediated redox modulation, Nat. Chem. Biol. 7 (2011) 588–590.
[20] J. Horsch, P. Wilke, M. Pretzler, M. Seuss, I. Melnyk, D. Remmler, A. Fery, A. Rompel, H.G. Börner, Polymerizing like mussels do: toward synthetic mussel foot proteins and resistant glues, Angew. Chem. 130 (2018) 15954–15958.
[21] Y.J. Xu, K. Wei, P. Zhao, Q. Feng, C.K.K. Choi, L. Bian, Preserving the adhesion of catechol-conjugated hydrogels by thiourea–quinone coupling, Biomaterials science 4 (2016) 1726–1730.
[22] K. Wei, B. Senturk, M.T. Matter, X. Wu, I.K. Herrmann, M. Rottmar, C. Toncelli, Mussel-inspired injectable hydrogel adhesive formed under mild conditions features near-native tissue properties, ACS Appl. Mater. Interfaces 11 (2019) 47707–47719.
[23] C. Shao, M. Wang, L. Meng, H. Chang, B. Wang, F. Xu, J. Yang, P. Wan, Mussel-inspired cellulose nanocomposite tough hydrogels with synergistic self-healing, adhesive, and strain-sensitive properties, Chem. Mater. 30 (2018) 3110–3121.
[24] M. Shin, E. Park, H. Lee, Plant-inspired pyrogallol-containing functional materials, Adv. Funct. Mater. 29 (2019) 1903022.
[25] K. Liu, L. Han, P. Tang, K. Yang, D. Gan, X. Wang, K. Wang, F. Ren, L. Fang, Y. Xu, An anisotropic hydrogel based on mussel-inspired conductive ferrofluid composed of electromagnetic nanohybrids, Nano Lett. 19 (2019) 8343–8356.
[26] M. Patenaude, N.M. Smeets, T. Hoare, Designing injectable, covalently cross-linked hydrogels for biomedical applications, Macromol. Rapid Commun. 35 (2014) 598–617.
[27] V. Kumar, J.T. Harris, A. Ribbe, M. Franc, Y. Bae, A.J. McNeil, S. Thayumanavan, Construction from destruction: hydrogel formation from triggered depolymerization-based release of an enzymatic catalyst, ACS Macro Lett. 9 (2020) 377–381.
[28] X. Wang, S. Chen, D. Wu, Q. Wu, Q. Wei, B. He, Q. Lu, Q. Wang, Oxidoreductase-initiated radical polymerizations to design hydrogels and micro/nanogels: mechanism, molding, and applications, Adv. Mater. 30 (2018) 1705668.
[29] X. Wu, H. Yue, Y. Zhang, X. Gao, X. Li, L. Wang, Y. Cao, M. Hou, H. An, L. Zhang, Packaging and delivering enzymes by amorphous metal-organic frameworks, Nat. Commun. 10 (2019) 1–8.
[30] W. Kang, T. Ma, M. Liu, J. Qu, Z. Liu, H. Zhang, B. Shi, S. Fu, J. Ma, L.T.F. Lai, Modular enzyme assembly for enhanced cascade biocatalysis and metabolic flux, Nat. Commun. 10 (2019) 1–11.
[31] J. Wu, X. Wang, Q. Wang, Z. Lou, S. Li, Y. Zhu, L. Qin, H. Wei, Nanomaterials with enzyme-like characteristics (nanozymes): next-generation artificial enzymes (ii), Chem. Soc. Rev. 48 (2019) 1004–1076.
[32] Q. Liang, J. Xi, X.J. Gao, R. Zhang, Y. Yang, X. Gao, X. Yan, L. Gao, K. Fan, A metal-free nanozyme-activated prodrug strategy for targeted tumor catalytic therapy, Nano Today 35 (2020) 100935.
[33] Y. Yang, D. Zhu, Y. Liu, B. Jiang, W. Jiang, X. Yan, K. Fan, Platinum-carbon-integrated nanozymes for enhanced tumor photodynamic and photothermal therapy, Nanoscale 12 (2020) 13548–13557.
[34] L. Gao, J. Zhuang, L. Nie, J. Zhang, Y. Zhang, N. Gu, T. Wang, J. Feng, D. Yang, S. Perrett, Intrinsic peroxidase-like activity of ferromagnetic nanoparticles, Nat. Nanotechnol. 2 (2007) 577–583.
[35] R. Zhang, K. Fan, X. Nanozymes Yan, Created by learning from nature, Sci. China Life Sci. 63 (2020) 1183–1200.
[36] Q. Tang, S. Cao, T. Ma, X. Xiang, H. Luo, P. Borovskikh, R.D. Rodriguez, Q. Guo, L. Qiu, C. Cheng, Engineering biofunctional enzyme-mimics for catalytic therapeutics and diagnostics, Adv. Funct. Mater. (2020) 2007475.
[37] L. Ma, F. Jiang, X. Fan, L. Wang, C. He, M. Zhou, S. Li, H. Luo, C. Cheng, L. Qiu, Metal–organic-framework-engineered enzyme-mimetic catalysts, Adv. Mater. (2020) 2003065.
[38] D. Jiang, D. Ni, Z.T. Rosenkrans, P. Huang, X. Yan, W. Cai, Nanozyme: new horizons for responsive biomedical applications, Chem. Soc. Rev. 48 (2019) 3683–3704.
[39] R. Yan, S. Sun, J. Yang, W. Long, J. Wang, X. Mu, Q. Li, W. Hao, S. Zhang, H. Liu, Nanozyme-based bandage with single-atom catalysis for brain trauma, ACS Nano 13 (2019) 11552–11560.
[40] J. Lian, D. Yin, S. Zhao, X. Zhu, Q. Liu, X. Zhang, X. Zhang, Core-shell structured Ag-coo nanoparticles with superior peroxidase-like activity for colorimetric sensing hydrogen peroxide and O-phenylenediamine, Colloid. Surface. Physicochem. Eng. Aspect. (2020) 125283.
[41] Y. Liu, J. Wang, X. Song, K. Xu, H. Chen, C. Zhao, J. Li, Colorimetric immunoassay for Listeria monocytogenes by using core gold nanoparticles, silver nanoclusters as oxidase mimetics, and aptamer-conjugated magnetic nanoparticles, Microchimica Acta 185 (2018) 360.
[42] Y. Sang, W. Li, H. Liu, L. Zhang, H. Wang, Z. Liu, J. Ren, X. Qu, Construction of nanozyme-hydrogel for enhanced capture and elimination of bacteria, Adv. Funct. Mater. 29 (2019) 1900518.
[43] Y. Hao, Y. Liu, Y. Wu, N. Tao, D. Lou, J. Li, X. Sun, Y.-N. Liu, A robust hybrid nanozyme@ hydrogel platform as a biomimetic cascade bioreactor for combination antitumor therapy, Biomaterials Science 8 (2020) 1830–1839.
[44] S. Zhao, H. Duan, Y. Yang, X. Yan, K. Fan, Fenozyme protects the integrity of the blood–brain barrier against experimental cerebral malaria, Nano Lett. 19 (2019) 8887–8895.
[45] W. Han, B. Zhou, K. Yang, X. Xiong, S. Luan, Y. Wang, Z. Xu, P. Lei, Z. Luo, J. Gao, Biofilm-inspired adhesive and antibacterial hydrogel with tough tissue integration performance for sealing hemostasis and wound healing, Bioactive Materials 5 (2020) 768–778.
[46] N. Wang, Q. Sun, J. Yu, Ultrasmall metal nanoparticles confined within crystalline nanoporous materials: a fascinating class of nanocatalysts, Adv. Mater. 31 (2019) 1803966.
[47] B.H. Kim, M.J. Hackett, J. Park, T. Hyeon, Synthesis, characterization, and application of ultrasmall nanoparticles, Chem. Mater. 26 (2014) 59–71.
[48] D. Gan, W. Xing, L. Jiang, J. Fang, C. Zhao, F. Ren, L. Fang, K. Wang, X. Lu, Plant-inspired adhesive and tough hydrogel based on Ag-lignin nanoparticles-triggered dynamic redox catechol chemistry, Nat. Commun. 10 (2019) 1–10.

[49] Z. Jia, Y. Zeng, P. Tang, D. Gan, W. Xing, Y. Hou, K. Wang, C. Xie, X. Lu, Conductive, tough, transparent, and self-healing hydrogels based on catechol–metal ion dual self-catalysis, Chem. Mater. 31 (2019) 5625–5632.
[50] I.S. Chae, S.W. Kang, J.Y. Park, Y.G. Lee, J.H. Lee, J. Won, Y.S. Kang, Surface energy-level tuning of silver nanoparticles for facilitated olefin transport, Angew. Chem. 123 (2011) 3038–3041.
[51] H. Choi, J.H. Lee, Y.R. Kim, D. Song, S.W. Kang, S.S. Lee, Y.S. Kang, Tetrathiafulvalene as an electron acceptor for positive charge induction on the surface of silver nanoparticles for facilitated olefin transport, Chem. Commun. 50 (2014) 3194–3196.
[52] I.S. Chae, S.W. Kang, J.Y. Park, Y.-G. Lee, J.H. Lee, J. Won, Y.S. Kang, Surface energy-level tuning of silver nanoparticles for facilitated olefin transport, Angew. Chem. Int. Ed. 50 (2011) 2982–2985.
[53] J.M. Brandner, S. Zacheja, P. Houdek, I. Moll, R. Lobmann, Expression of matrix metalloproteinases, cytokines, and connexins in diabetic and nondiabetic human keratinocytes before and after transplantation into an ex vivo wound-healing model, Diabetes Care 31 (2008) 114–120.
[54] P. Casuso, I. Odriozola, A. Pérez-San Vicente, I. Loinaz, G. Cabañero, H.-J. Grande, D. Dupin, Injectable and self-healing dynamic hydrogels based on metal(I)-Thiolate/Disulfide exchange as biomaterials with tunable mechanical properties, Biomacromolecules 16 (2015) 3552–3561.
[55] H. Chen, R. Cheng, X. Zhao, Y. Zhang, A. Tam, Y. Yan, H. Shen, Y.S. Zhang, J. Qi, Y. Feng, L. Liu, G. Pan, W. Cui, L. Deng, An injectable self-healing coordinative hydrogel with antibacterial and angiogenic properties for diabetic skin wound repair, NPG Asia Mater. 11 (2019) 3.
[56] G. Fang, W. Li, X. Shen, J.M. Perez-Aguilar, Y. Chong, X. Gao, Z. Chai, C. Chen, C. Ge, R. Zhou, Differential Pd-nanocrystal facets demonstrate distinct antibacterial activity against gram-positive and gram-negative bacteria, Nat. Commun. 9 (2018) 1–9.
[57] A. Chiloeches, C. Echeverría, R. Cuervo-Rodríguez, D. Plachà, F. López-Fabal, M. Fernández-García, A. Muñoz-Bonilla, Adhesive antibacterial coatings based on copolymers bearing thiazolium cationic groups and catechol moieties as robust anchors, Prog. Org. Coating 136 (2019) 105272.
[58] W.-R. Li, X.-B. Xie, Q.-S. Shi, H.-Y. Zeng, O.-Y. You-Sheng, Y.-B. Chen, Antibacterial activity and mechanism of silver nanoparticles on Escherichia coli, Appl. Microbiol. Biotechnol. 85 (2010) 1115–1122.
[59] W. Zhang, R. Wang, Z. Sun, X. Zhu, Q. Zhao, T. Zhang, A. Cholewinski, F. Yang, B. Zhao, R. Pinnaratip, P.K. Forooshani, B.P. Lee, Catechol-functionalized hydrogels: biomimetic design, adhesion mechanism, and biomedical applications, Chem. Soc. Rev. 49 (2020) 433–464.
[60] P. Kord Forooshani, B.P. Lee, Recent approaches in designing bioadhesive materials inspired by mussel adhesive protein, J. Polym. Sci. Polym. Chem. 55 (2017) 9–33.
[61] L. Han, X. Lu, K. Liu, K. Wang, L. Fang, L.-T. Weng, H. Zhang, Y. Tang, F. Ren, C. Zhao, Mussel-inspired adhesive and tough hydrogel based on nanoclay confined dopamine polymerization, ACS Nano 11 (2017) 2561–2574.
[62] H.R. Culver, M.E. Wechsler, N.A. Peppas, Label-free detection of tear biomarkers using hydrogel-coated gold nanoshells in a localized surface plasmon resonance-based biosensor, ACS Nano 12 (2018) 9342–9354.
[63] Y.S. Kang, S.W. Kang, H. Kim, J.H. Kim, J. Won, C.K. Kim, K. Char, Interaction with olefins of the partially polarized surface of silver nanoparticles activated by P-benzoquinone and its implications for facilitated olefin transport, Adv. Mater. 19 (2007) 475–479.
[64] D. Gan, Z. Huang, X. Wang, L. Jiang, C. Wang, M. Zhu, F. Ren, L. Fang, K. Wang, C. Xie, X. Lu, Graphene oxide-templated conductive and redox-active nanosheets incorporated hydrogels for adhesive bioelectronics, Adv. Funct. Mater. 30 (2020) 1907678.